Long-term stochastic heave-induced dynamic buckling of a top-tensioned riser and its influence on the ultimate limit state reliability

José Manuel Cabrera-Miranda [a,b] and Jeom Kee Paik [a,b,c,*]

[a] *Department of Naval Architecture and Ocean Engineering, Pusan National University, Busan 46241, Republic of Korea*

[b] *The Korea Ship and Offshore Research Institute (The Lloyd's Register Foundation Research Centre of Excellence), Pusan National University, Busan 46241, Republic of Korea*

[c] *Department of Mechanical Engineering, University College London, London WC1E 7JE, UK*

** Corresponding Author. J.K. Paik. Tel: +82 51 510 2429, Mobile: +82 10 3853 8757, Fax: +82 51 518 7687*

E-mail addresses: cabrera@pusan.ac.kr (J.M. Cabrera-Miranda), jeompaik@pusan.ac.kr (J.K. Paik).

Abstract

A top-tensioned riser is a slender pipe that conveys fluids between a floater and a subsea system. High top-tension keeps its straight configuration and helps to prevent compressive loads. Because of the floater's heave motion, the tension on the riser fluctuates giving rise to dynamic buckling. This paper examines the dynamic buckling characteristics of a top-tensioned riser analyzing the governing equation with nonlinear damping. The equation is discretized in space by the finite difference method and then is numerically integrated by the Runge-Kutta method. As main objective, an ultimate limit state function for risers is used to investigate its reliability during parametric excitation. While the short-term stationary Gaussian random motion of a floater can be described by a response spectrum, the uncertainties of a long-term response are considered by Monte Carlo simulation. In view of an applied example, it is found that the dynamic buckling would occur often, and although the probability of failure is acceptable, it can cause serious failure when axial excitation is of significance in harsher sea states. This study aims to contribute in clarifying the role of parametric vibrations (dynamic buckling) in the reliability of risers for ultimate limit state.

Keywords: marine riser; random heave-induced parametric excitation; nonlinear quadratic damping; probability of dynamic buckling; ultimate limit state reliability analysis.

1. Introduction

A top-tensioned riser (hereafter referred to solely as a riser throughout this paper) consists of a vertical pipe, which is used in the offshore industry to convey drilling fluids, oil, gas, water or chemicals from its respective floater to a subsea system or vice versa. This type of structure is mostly used in deep water, where the relative motion between the floater and the subsea system is minor.

One of the technical challenges in the application of risers is the occurrence of heave-induced parametric excitation which may lead to dynamic buckling. A riser is held at its top end by a tensioning system, which keeps the riser's body under tension in order to avoid compressive loads; nevertheless, due to the floater's heave (vertical motion), the tension fluctuates with time, and lateral vibrations (dynamic buckling) can be excited. The unwanted consequence us such phenomenon is the riser's damage due to excessive stress which could lead to oil or gas spills with consequent pollution and economic loses (Yang et al., 2013). Moreover, it is known that the heave motions of floaters are responsible for bending and buckling conditions that can lead to fatigue damage of risers (Katifeoglou and Chatjigeorgiou, 2016).

From the cost perspective, it would be desirable to reduce the tensioning capacity and to permit the riser to operate in low tension (Patel and Vaz, 1996), nonetheless large heave motions can cause serious damage to the riser and thus it is necessary to balance the capital with the risk expenditures in order to optimize the riser's design and operations. To give idea of the consequences, the World Offshore Accident Database (DNV GL, 2016) has reported at least 2 accidents related to the partition of marine drilling risers during stormy conditions with large heave motions

where the largest consequence is spill of drilling mud to sea, 1 accident where the drilling string broke after the maximum deflection of the heave compensator was reached, and 4 accidents where one riser tensioner wired failed. Unfortunate events as the above mentioned, can be avoided if inadequacies are solved at design stage, being the most common ones (Patel and Witz, 1991, Chapter 11): failure to predict multiple curvature, failure to predict high curvature, inadequate top-tension availability, inadequate tensioner rate, excessive bending in free-hanging condition and failure of buoyancy modules.

Regarding the description of dynamic buckling, the amplitude of the response is often larger near the bottom owing to the spatial variation of tension with depth. It can be excited via three main mechanisms (Kuiper et al., 2008). First, classic parametric resonance may develop when the frequency and amplitude of the floater's heave excite a specific riser mode or combination of modes. In this situation, the response frequency is about twice the excited eigen-frequency (Park and Jung, 2002), also as confirmed by experiments (Franzini et al., 2015). Second, sub-critical buckling can arise when the floater heaves with low frequency and large amplitude, and thus a single wave grows near the riser's bottom and then propagates along its length. Third, when frequency and amplitude are high enough, buckling waves are generated periodically near the bottom, travel and decompose in a combination of riser modes.

Many studies have been devoted to the issue of parametric excitation of offshore structures in which a coefficient appears as function of time in the governing differential equation. Said studies have included the research about risers and cables (Chatjigeorgiou, 2004; Chatjigeorgiou and Mavrakos, 2005, 2002; Franzini et al., 2015;

Franzini and Mazzilli, 2016; Hsu, 1975; Kuiper et al., 2008; Lei et al., 2014; Mazzilli et al., 2016; Park and Jung, 2002; Prado et al., 2014; Wang et al., 2015; Wu et al., 2016; Xiao and Yang, 2014; Yang et al., 2013; Yang and Xiao, 2014; Zhang and Tang, 2015), tethers for tension-leg platforms (Patel and Park, 1995, 1991), submerged floating pipelines (Yang et al., 2017) and parametric rolling of ships (Pipchenko, 2009; Thomas et al., 2010).

The general approach to investigate the parametric excitation of risers and tethers is as follows: (1) First, the nonlinear governing equation of motion with a time-dependent coefficient is derived. (2.a) Then the stability of the linear Mathieu's equation (for single-frequency excitation) (Chatjigeorgiou and Mavrakos, 2002; Hsu, 1975; Park and Jung, 2002; Patel and Park, 1995, 1991; Prado et al., 2014; Wang et al., 2015) or Hill's equation (for multi-frequency excitation) (Xiao and Yang, 2014; Yang et al., 2013) is analyzed via the Strutt's diagram, where the stability is estimated analytically. (2.b) Another alternative is to analyze the linearized system by means of the Floquet theory (Kuiper et al., 2008; Lei et al., 2014; Zhang and Tang, 2015). (3) Finally, the nonlinear equation is solved in the time-domain to examine the effect of nonlinear terms (Chatjigeorgiou and Mavrakos, 2002) and the map of the steady-state amplitude can be plotted (Franzini and Mazzilli, 2016; Kuiper et al., 2008; Mazzilli et al., 2016; Prado et al., 2014).

Some variations of the analysis consist of adding forced vibrations, such as surge (horizontal) motions at the top end of the riser. Scholars have found that the response period of combined parametric and forcing excitation is dependent on the relative strengths of each type of excitation (Patel and Park, 1995). The finite element

method in order to address axial and torsional effects, and results have shown that the responses of combined excitations can be in general equal or larger than for surge forcing excitation alone (Park and Jung, 2002). Another study that used small deformation theory, found that the bending stresses on top-tensioned risers increase as the amplitude of floater's drift motion increase, especially at the bottom end of the riser (Li et al., 2010). On the other hand, the frequency of said motion has dominant effect on the stresses at the upper part. Other researchers have investigated parametric excitation of risers have included other phenomena such as sea wave forces (Lei et al., 2014; Wu et al., 2016), vortex-induced vibrations (Wang et al., 2015; Yang and Xiao, 2014) and earthquake excitation (Wu et al., 2016).

A couple of experiments have been reported in the literature. The first one (Franzini et al., 2015) used spectral analysis of the experiments and Strutt diagrams to investigate the response at different frequency ratios of top excitation to eigen frequency. The second (Mazzilli et al., 2016) used the Galerkin method with Bessel functions to solve the riser's motion numerically and compared the results against experimental data.

The present paper focuses on the investigation whether the random heave-induced dynamic buckling can lead to structural failure of a riser in the long-term. While useful methods and findings are available in the literature, there are some differences that might be highlighted for this study. (1) The riser's response due to the random floater's motion is investigated, while previous studies have focused either on the floater's harmonic motion or have assumed that the riser's top end follows the random sea surface. (2) Realistic probability density functions (PDFs) are employed to describe

the long-term statistics of sea waves which are input for the reliability analysis. (3) Moreover, Monte Carlo simulation (MCS) is performed to assess the probability of dynamic buckling and the probability of failure after dynamic buckling, which up to the authors' knowledge have not been evaluated in the past.

The description of the paper is presented comprising six sections. After Section 1 for introduction, Section 2 presents the governing equation of a riser and its discretization by means of the finite difference into a system of nonlinear ordinary differential equations. Section 3 identifies combinations of significant wave height and wave spectral peak circular frequency that lead to dynamic buckling, where the dynamic stability of the riser is first analyzed and then a map of maximum amplitude response is used. In Section 4, the MCS method is introduced and then applied for the structural reliability analysis of a riser in Section 5. Finally, insights and findings from the present study are addressed in Section 6.

2. Mathematical model

2.1 Governing equation

The straight vertical riser submerged in a fluid medium is considered as shown in Fig. 1. The tensioning system is approximated as a soft spring k_1, and the flexible joints as rotational springs k_2 and k_3.

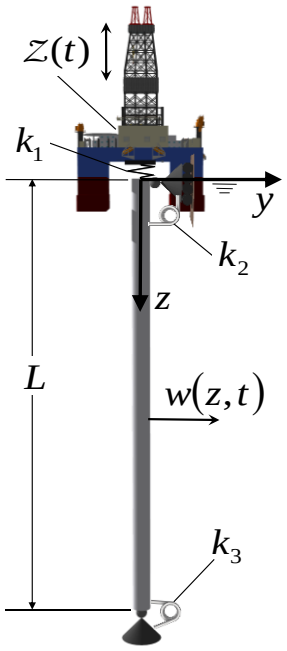

Fig. 1 Sketch of a top-tensioned riser with a floater's heave-induced excitation.

Under the small-deformation theory of columns (Paik and Thayamballi, 2003, Chapter 9), and including the fluid's drag damping, the in-plane governing equation for a riser surrounded by quiescent water can be expressed as

$$EI\frac{\partial^4 w}{\partial z^4}-\frac{\partial}{\partial z}\left[T_e\left(z,t\right)\frac{\partial w}{\partial z}\right]+M\frac{\partial^2 w}{\partial t^2}+\frac{1}{2}C_d\rho_f D\left|\frac{\partial w}{\partial t}\right|\frac{\partial w}{\partial t}=0, \quad (1)$$
$$0\le z\le L,$$

subjected to the boundary conditions

$$
\begin{aligned}
&w(0,t)=0,\\
&\left.\frac{\partial^2 w(z,t)}{\partial z^2}\right|_{z=0}=\frac{k_2}{EI}\left.\frac{\partial w(z,t)}{\partial z}\right|_{z=0},\\
&w(L,t)=0,\\
&\left.\frac{\partial^2 w(z,t)}{\partial z^2}\right|_{z=L}=-\frac{k_3}{EI}\left.\frac{\partial w(z,t)}{\partial x}\right|_{z=L},
\end{aligned}
\tag{2}
$$

where $w(z,t)$ is the lateral displacement of a riser as a function of depth z and time t, E is the Young's Modulus, I is the area moment of inertia of a riser, T_e is the effective tension, M is the mass per unit length which includes the riser's solid body, internal fluid and added mass, C_d is the drag coefficient, ρ_f is the surrounding fluid's density (seawater), D is the outer diameter of the riser for drag force calculations, and L is the riser's length.

2.2 Description of time-varying tension

The effective tension of a riser is derived from the rod equation, subjected to the spring force at $z=0$, and zero displacement at $z=L$. By assuming quasi-static response, the effective tension reads

$$
T_e(z,t)=W_e fL-W_e z-k_1 \mathcal{Z}(t), \tag{3}
$$

where W_e is the submerged weight of a riser per unit length, f is the pretension factor, and $\mathcal{Z}(t)$ is the floater's heave motion. The first term is the applied static tension to the riser's top end, while the second accounts for the riser's self-weight, internal fluid's weight and buoyancy.

Concerning the third term in Eq. (3), the sea waves excite the floater, and in turn the floater excites the riser, yielding in a time-varying tension. The sea waves are described by their variance density spectrum $\mathrm{S}(\omega)$, where ω is the circular frequency of the waves. The floater's heave motion is characterized by its heave transfer function or response amplitude operator $\mathrm{RAO}(\omega)$ (time-invariant linear relationship between the sea wave amplitude and response amplitude). Then, the heave response spectrum can be computed as follows (Det Norske Veritas AS, 2014):

$$\mathrm{RS}_{\mathcal{Z}}(\omega) = \left|\mathrm{RAO}(\omega)\right|^2 \mathrm{S}(\omega). \tag{4}$$

Adopting a random-phase/amplitude model, the random heave response in time-domain can be computed as the summation of harmonic heave waves, i.e.

$$\mathcal{Z}(t) = -\sum E\{\underline{a}_i\}\cos(\omega_i t + \underline{\varepsilon}_i), \forall i, \tag{5}$$

where $E\{\cdot\}$ indicates expectation, the underscore denotes a random variable, $\underline{a}_i$ is the random heave amplitude for the i-th frequency ω_i, $E\{\underline{a}_i\} = \sqrt{2\mathrm{RS}_{\mathcal{Z}}(\omega_i)\Delta\omega}$ is the amplitude spectrum evaluated at ω_i, $\Delta\omega$ is the circular frequency increment and $\underline{\varepsilon}_i$ is the random phase uniformly distributed between $-\pi$ and π.

To obtain the remaining terms, the spring constant is given as follows (Kuiper et al., 2008):

$$k_1 = \not{k}\, LW_e / a_c, \tag{6}$$

where a_c is the floater's critical heave amplitude, and the factor k_c has been introduced in order to take into account the uncertainty. This formulation is consistent with the simplified tensioner model 1 in ISO 13624-2 (ISO, 2009).

At last, the pretension factor is calculated as follows:

$$f = F\, T_m / LW_e, \tag{7}$$

where T_m is the minimum allowable top-tension as defined in API RP 16Q (American Petroleum Institute, 2017) and F is a factor which must be positive to comply with the said guidelines.

2.3 Numerical solution

To solve Eq. (1), the space is discretized by means of the finite difference method with central difference approximation. The derivation is presented in the Appendix A.

Writing the finite difference equations into state-space form, gives a system ordinary nonlinear differential equations, which in this study are solved by the Runge-Kutta-Fehlberg method. This is a 4th-5th order Runge-Kutta procedure with optimum-adaptive step size available in Matlab as ode45 differential equation solver. Throughout the paper, this method is referred to as time-domain analysis. By this approach, the analysis of dynamic buckling response takes roughly 7 minutes to simulate 4.5 hours of a sea state, with 53 nodes, in a computer with processor Intel(R) Core(TM) i5-4590 CPU @ 3.30GHz 8.00 GB installed memory (RAM).

3 Map of dynamic buckling

3.1 Properties of a riser

Stability analysis is carried out and then the maximum absolute response map is computed for a marine drilling riser made of X-80-grade steel 21 in (533.4 mm) main conductor with properties taken from the literature (Permana, 2012) (see Table 1). Linear regression is applied to approximate M, W_e and T_m as functions of the internal fluid's density ρ_i. In this section, $k_c = F$ =1 and ρ_i =1 600 kg·m^{-3} are taken, unless otherwise indicated.

Table 1 Properties of a riser

Property	Value
E	2.1×10^{11} N·m^{-2}
I	1.17×10^{-3} m^4
C_a	1
C_d	0.8
M	$(1+C_a)(0.2164\,\rho_i+1155.2)$ kg·m^{-1}
ρ_f	1025 kg·m^{-3}
D	1.4224 m
L	3000 m
W_e	$2.1225\,\rho_i$-2305.5 N·m^{-1}
a_c	10 m
k_2	5 × 10^5 N·m·rad^{-1}
k_3	5 × 10^6 N·m·rad^{-1}
T_m	$8480\,\rho_i$-7.43×10^6 N

As a target floater, a semi-submersible with properties used in a previous study (Cabrera-Miranda and Paik, 2017) is considered and the heave RAO for head waves (traveling in longitudinal direction) is calculated analytically (Clauss et al., 1992) [see Fig. 2(a)]. Only sea waves for the said direction are considered in this study for simplicity of problems. Moreover, the JONSWAP formulation (Det Norske Veritas AS, 2014) is used to compute the sea waves' variance density spectrum as a function of the significant wave height H_S (mean of the highest one-third of waves in a wave record) and the spectral peak circular frequency ω_p. Alternatively, one may use the zero-crossing wave period T_Z (mean of the interval between one zero-down crossing of a wave and the next), as addressed in Section 5. The JONSWAP spectrum was selected over the Pierson-Moskowitz Spectrum because, as illustrated in Fig. 2(c), larger floater motions are produced with the former. Fig. 2(b) and (c) are generated by using the mean for $\underline{H}_S$ and $\underline{T}_Z$ introduced in Section 5.

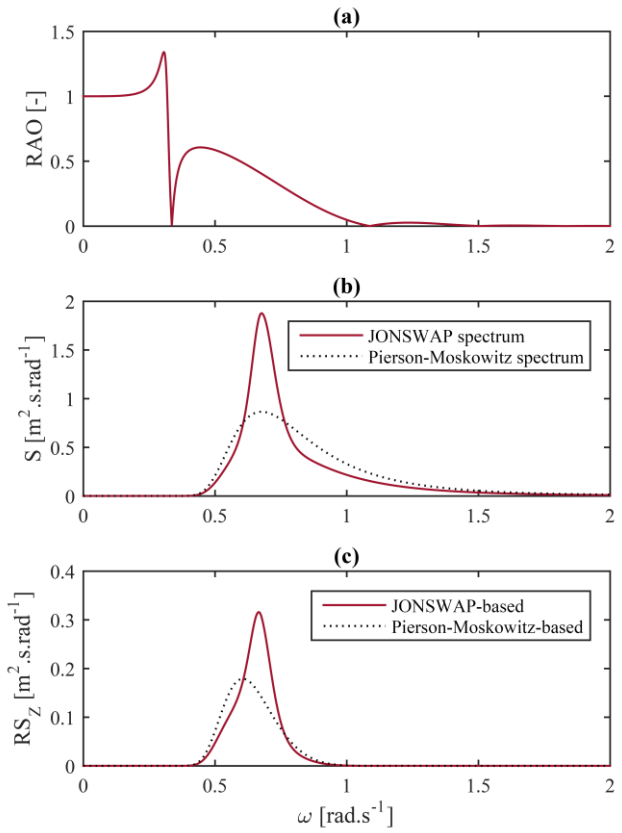

Fig. 2 (a) Response amplitude operator of floater's heave, (b) wave variance density spectra and (c) heave response spectra for H_S=2.5567 m and ω_p=0.6768 rad·s^{-1}.

3.2 Lyapunov stability analysis and nonlinear damping stabilization

Following the strategy for the analysis from previous researchers, it is attempted to compute the stability map of the riser response. It is noted that the system of finite difference equations [Eq. (A7)] represents a nonlinear dynamical system which stability can be defined by means of the Lyapunov exponents (Nayfeh and Balachandran, 2004, Chapter 7). Lyapunov exponents are measures of mean exponential rate of divergence of small perturbations to the solutions of a dynamical system (Benettin et al., 1980a; Lu

et al., 2005). Stable dynamical systems have negative Lyapunov exponents, whereas chaotic systems have one or more positive Lyapunov exponents.

By using the method developed by Shimada and Nagashima (1979) and Benettin et al. (1980a, 1980b), the Lyapunov exponents of the nonlinear system are computed for a few cases. As an example, Fig. 3 illustrates the results for a sea state (random process) where dynamic buckling occurs, where η is the dimensionless transverse deflection, τ is the dimensionless time and ξ is the dimensionless coordinate, all defined in the Appendix A.

As initial conditions, a half-wave deformation $\eta(\xi,0)=\tilde{\eta}\sin(\xi\pi)$ is prescribed with amplitude $\tilde{\eta}$ =0.00001. Figs. 3(a) and 3(c) show that the initial conditions impose a quasi-periodic transient motion which remains for part of the simulation. Then, the response grows bounded by the quadratic damping. Fig. 3(b) represents the evolution of the first 5 Lyapunov exponents, which are all negative and hence it is concluded that the system is stable or non-chaotic.

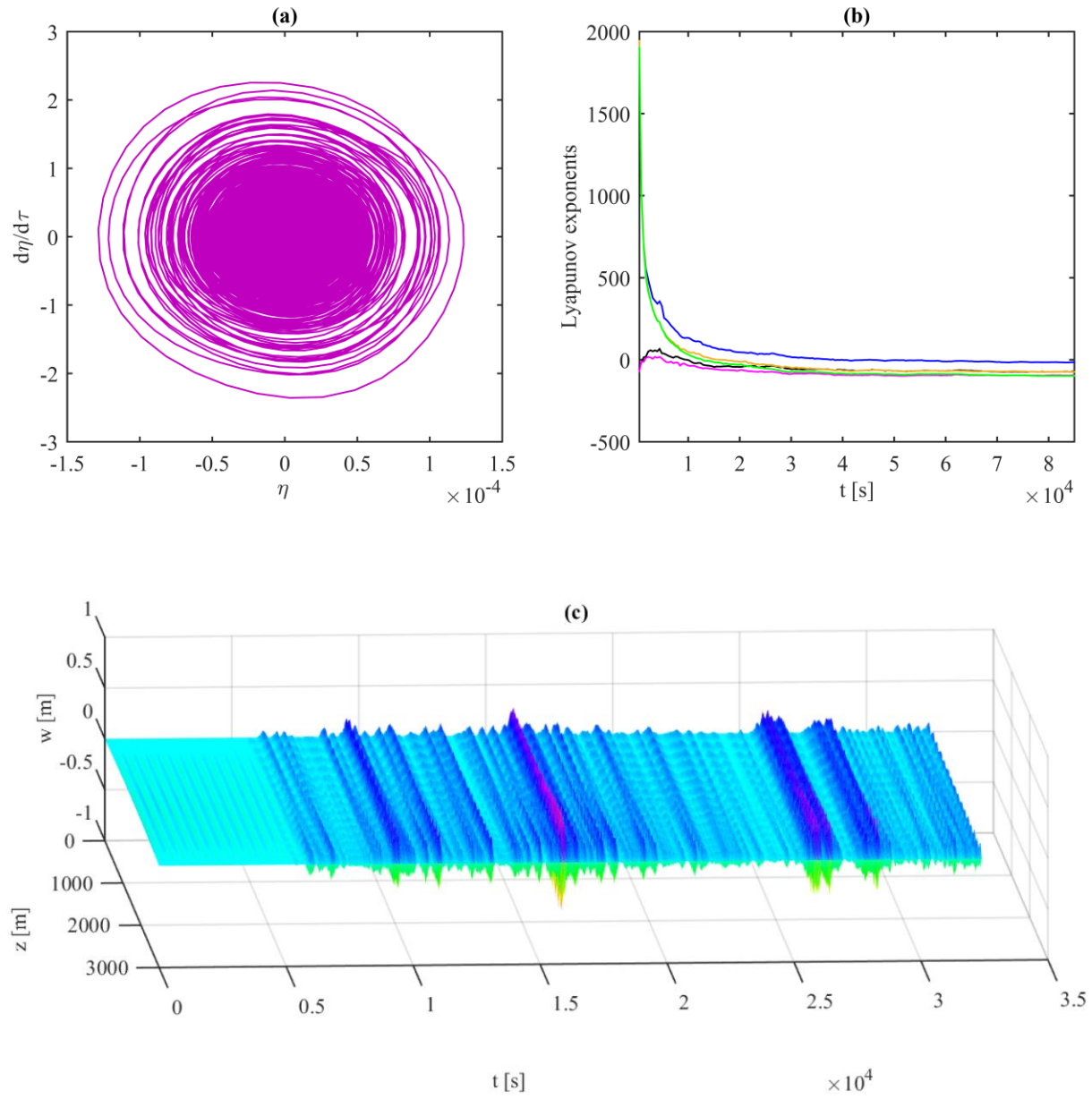

Fig. 3 Evolution of dynamic buckling for H_S =10.13 m, ω_p =0.3972 rad·s^{-1}: (a) phase portrait of riser motion at ξ =0.8846, (b) time history of highest 5 Lyapunov exponents and (c) time history of transverse deflection.

Some unstable combinations of parameters are possible for the finite difference riser equations. For instance, using same parameters as for Fig. 3, but with k_c=100 which amplifies the heave excitation, the first Lyapunov exponent is 3242 and at least the next four are positive. Therefore, the system becomes unstable; nevertheless, one may not be interested in high k_c values for riser applications.

In summary, the presence of drag damping stabilizes the riser's motion whenever dynamic buckling occurs, which is not a surprising finding since this is the case for most parametrically excited systems, where nonlinearities limit the growth of the response (Nayfeh and Mook, 1985, Chapter 5). This finding is also in agreement with other works that have studied the parametric vibrations of the riser with quadratic damping (Chatjigeorgiou and Mavrakos, 2002; Franzini and Mazzilli, 2016; Kuiper et al., 2008; Mazzilli et al., 2016; Patel and Park, 1995). The hydrodynamic damping is the decrease of amplitude of small oscillations of a body by forces in anti-phase with velocity, which in turn are caused by oscillations of the boundary layer that give rise to skin friction, normal pressure and complex coherent and quasi-coherent fluid structures (Sarpkaya, 2010, Chapter 7).

3.3 Map of maximum response

As seen in the previous section, the concepts of dynamic stability and stability map are ineffective for the nonlinear riser equation in the domain of interest. Instead, a map of maximum absolute dynamic buckling response provides a pragmatic approach to identify sea parameters that may lead to dynamic buckling.

Fig. 4 displays the maximum riser deflection as a function of ω_p and H_S for a mesh of 100×100 points. The amplitude of the half-wave initial deformation is set to $\tilde{\eta}$ =0.00001. While each simulation time comprises 4.5 hours of response, only the last 3 hours were taken into account in order to let the effect of the initial conditions get dissipated. It is observed that dynamic buckling occurs for low ω_p which is explained by the fact that the studied floater is not excited by high frequencies (see Fig. 2).

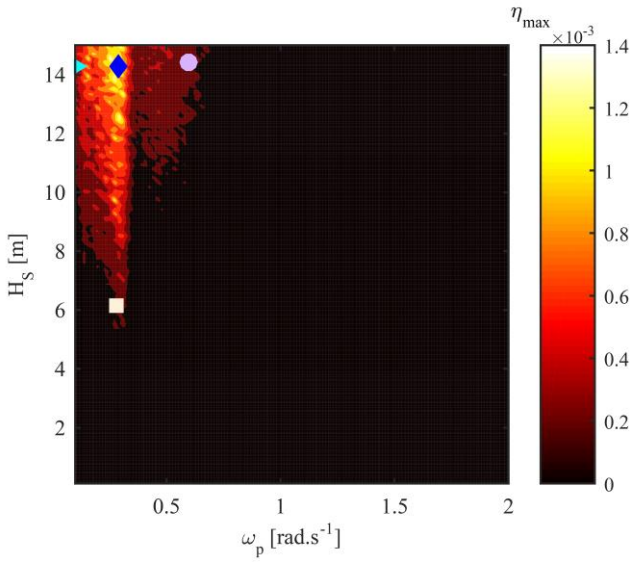

Fig. 4 Map of maximum absolute dynamic buckling response.

Fig. 5 presents an example for the response at four points in Fig. 4, which are indicated as a triangle, diamond, square and circle markers in the latter. It is noticed that the riser vibrates in a combination of standing wave pattern with some traveling waves. Furthermore, higher modes are excited as ω_p increases. For the case of lower

frequency as shown in Fig. 5(a), the maximum response does not develop at a specific depth, while for the other cases it clearly happens near to the bottom end of the riser.

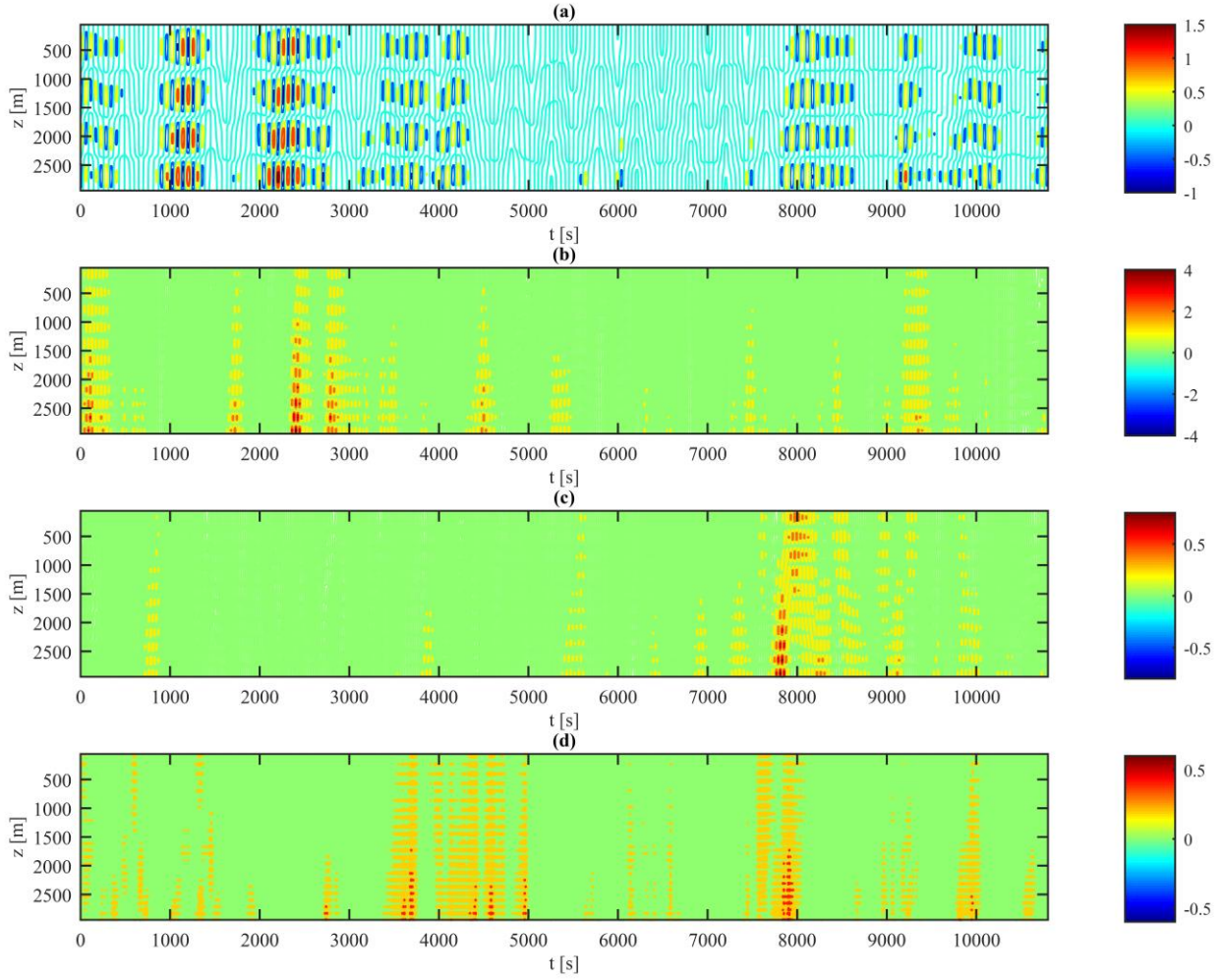

Fig. 5 Contours of the time history for transverse deflection [m] for (a) H_S =14.25 m, ω_p =0.11 rad·s^{-1}, (b) H_S =14.13 m, ω_p=0.2906 rad·s^{-1}, (c) H_S =6.13 m, ω_p=0.2843 rad·s^{-1}, (d) H_S =14.45 m, ω_p=0.5957 rad·s^{-1}.

4. Stochastic analysis

4.1 Probability of dynamic buckling

Based on the results of Section 4, it is realized that dynamic buckling is likely to happen in sea states of low wave frequency and high amplitude; nevertheless, one may be still interested in how often that event would happen and in whether such event can make the riser fail.

Concerning the probability of dynamic buckling, (i) the deformation imposed by the initial conditions will disappear in time if the riser finds the straight shape stability or (ii) it will grow until the quadratic damping stabilizes the system. Thus, the maximum buckling response relative to the initial deformation can be calculated as follows:

$$\eta_{rel}\left(\underline{\mathbf{X}}\right) = \max\left[\left|\eta\left(\xi,\tau,\underline{\mathbf{X}}\right)\right| - \eta_0 \sin\left(\xi\pi\right)\right], \forall\left(\xi,\tau\right) \in \left[0,1\right]\times\left[\tau_1,\tau_2\right], \tag{8}$$

where $\underline{\mathbf{X}}$ is the vector of long-term random variables, τ_1 is the initial time of the sea state, and τ_2 is the end time.

One should note that: $\eta_{rel} \le 0$ for situation (i) and $\eta_{rel} > 0$ for (ii). Since we are interested in (ii), here the probability of dynamic buckling is defined as follows:

$$P_B = \mathrm{P}\left\{\eta_{rel}\left(\underline{\mathbf{X}}\right) > 0\right\}, \tag{9}$$

where $\mathrm{P}\{\cdot\}$ denotes the probability.

4.2 Probability of structural failure

The calculation of the probability of failure for a system is a key task of the reliability analysis. To assess the structural reliability of the riser, local usage factors $u(\xi)$ for ultimate limit state can be calculated in the following form of (Det Norske Veritas, 2010):

$$u(\xi,\tau,\underline{\mathbf{X}})=\begin{cases}\sqrt{\dfrac{|\underline{\mathcal{M}}|}{\underline{\mathcal{M}}_k}\sqrt{1-\left(\dfrac{\underline{p}_i-p_e}{\underline{p}_b}\right)^2}+\left(\dfrac{\underline{T}_e}{\underline{T}_k}\right)^2+\left(\dfrac{\underline{p}_i-p_e}{\underline{p}_b}\right)^2}, & \underline{p}_i\geq p_e\\ \left\{\left[\dfrac{|\underline{\mathcal{M}}|}{\underline{\mathcal{M}}_k}+\left(\dfrac{\underline{T}_e}{\underline{T}_k}\right)^2\right]^2+\left(\dfrac{p_e-\underline{p}_i}{\underline{p}_c}\right)^2\right\}^{1/4}, & \underline{p}_i<p_e\end{cases} \tag{10}$$

where $\underline{\mathcal{M}}$ is the bending moment induced by the dynamic buckling, $\underline{\mathcal{M}}_k$ is the plastic bending moment resistance, $\underline{p}_i$ is the internal pressure, p_e is the external pressure, $\underline{p}_b$ is the burst resistance, $\underline{T}_k$ is the plastic axial force resistance and $\underline{p}_c$ is the hoop buckling capacity [for detailed definition of the variables, Det Norske Veritas (2010) is referred to].

Then, the global usage is given by

$$U(\underline{\mathbf{X}})=\max\left[u(\xi,\tau,\underline{\mathbf{X}})\right],\forall(\xi,\tau)\in[0,1]\times[\tau_1,\tau_2], \tag{11}$$

and the probability of failure can be computed as follows:

$$P_f=\mathrm{P}\left\{U(\underline{\mathbf{X}})\geq 1\right\}. \tag{12}$$

4.3 Monte Carlo simulation assisted by metamodels

The probabilities, Eq. (9) and Eq. (12) are computed in this study by means of Monte Carlo Simulation (MCS) (Zio, 2013). By this method, a random realization of the parameters $\underline{\mathbf{X}}$ correspond to each simulation (Forghani and Ritto, 2016).

In order to reduce the computational effort, a metamodel approach is implemented (Cabrera-Miranda and Paik, 2017; Garrè and Rizzuto, 2012; Xiao and Yang, 2014; Yang and Zheng, 2011). First, a sampling technique for design of experiments such as Latin hypercube sampling (LHS) is used to select a set of credible scenarios with limited number. Then, a time-domain dynamic analysis is carried out for the selected scenarios. Next, metamodels (approximate functions of $\underline{\mathbf{X}}$) are fed with the generated data and then used within the MCSs to estimate the output random variables $\underline{\eta}_{rel}$ and $\underline{U}$. At last, the limit state functions are evaluated to compute the probability of violating those limits, i.e. the number of simulations with buckling is counted and divided by the total number of simulations to find the probability of dynamic buckling; likewise, the probability of failure is calculated by dividing the number of simulations with failure by the total number of simulations.

The approximate time to perform the metamodel-assisted MCS is 54 minutes which requires memory for the storage of variables and metamodels. More time is spent in analyzing the LHS scenarios.

5. Applied example and discussion

Stochastic analysis is performed for a base case and then the influence of the minimum top-tension factor in the probability of dynamic buckling and failure is investigated. The riser and floater properties are the same as in Section 3.1. The procedure described in Fig. 6 is followed.

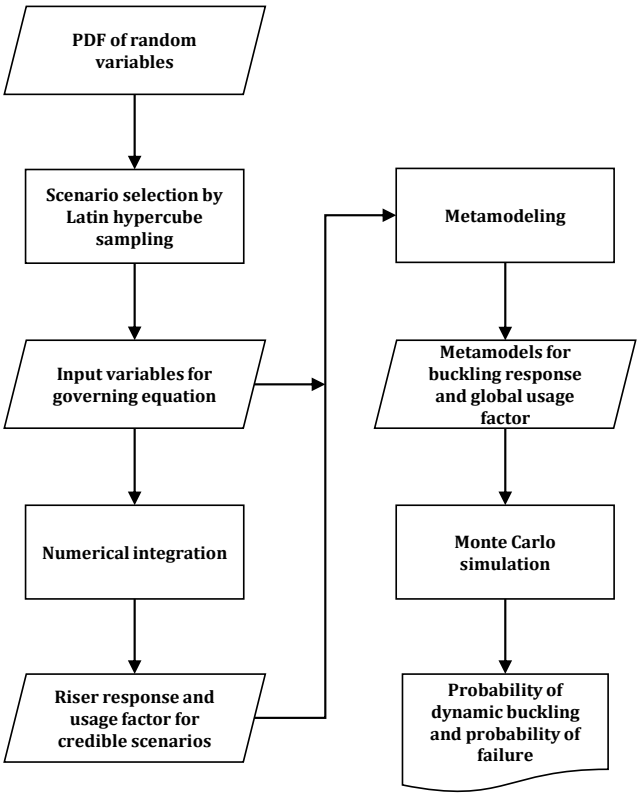

Fig. 6 Flowchart for calculating for calculating probability of dynamic buckling and probability of failure of a riser.

5.1 Base case

First, uncertainties in the environmental, functional conditions and strength variables are taken into account by means of their long-term PDFs as indicated in Table 2.

Table 2 Probabilistic distribution of long-term random variables for base case.

Variable	Description	Unit	Distribution	Reference
$\underline{H}_S$	significant wave height	m	Weibull (α=2.84, β=1.53)	Det Norske Veritas AS (2014), Area 4
$\underline{T}_Z$	Zero-crossing wave period	s	Log-normal (μ=0.07+1.125 $\underline{H}_S$ $^{0.15}$, σ=0.07+0.0978 exp (-0.0074 $\underline{H}_S$)	Det Norske Veritas AS (2014), Area 4
$\underline{\rho}_i$	internal fluid's density	kg·m^{-3}	Normal (μ=1527.5, σ=167.5)	Institut Français du Pétrole (1999) [a,b,c]
$\underline{k}$	Tensioning system stiffness factor	-	Normal (μ=1, σ=0.0333)	Assumed [a,b,d]
$\underline{F}$	Minimum tension factor	-	Normal (μ=1.15, σ=0.05)	Assumed [a,b,e]
$\underline{\sigma}_y$	Yield strength	Pa	Normal (μ=6.21×10^8, σ =1.242×10^7)	American Petroleum Institute (2004) [a,f]
$\underline{\sigma}_u$	Ultimate tensile strength	Pa	Normal (μ=7.24×10^8, σ =1.448×10^7)	American Petroleum Institute (2004) [a,f]

[a] Mean was estimated as $\mu = (x_{\max} + x_{\min})/2$, where $x_{\max}$ and $x_{\min}$ are the maximum and minimum values from the available data.

[b] Standard deviation was estimated as $\sigma = (x_{\max} - x_{\min})/6$ from available data

[c] Minimum value $x_{\min}$ is taken as seawater density

[d] $x_{\min}$ =0.9, $x_{\max}$ =1.1

[e] $x_{\min}$ =1, $x_{\max}$ =1.3

[f] 0.02 coefficient of variation (Kucheryavyi and Milkov, 2014)

Then, LHS is performed to choose 300 scenarios. This number is adequate for the computation Kriging metamodels for which 10 times the number of input variables are recommended to define the LHS size (Kleijnen, 2017); i.e. the minimum number of scenarios for 7 variables of this example is 70. The scenarios are analyzed in the time-domain for a total of 6 hours in order to let the transient response be dissipated and only data after 3 hours is further studied. Initial conditions are prescribed with $\tilde{\eta}$ =0.000001 and zero velocity. Next, the Blind-Kriging technique was used to construct Kriging metamodels by means of the ooDACE Matlab toolbox (Couckuyt et al., 2012, 2010; Ulaganathan et al., 2015), where the regression function is a polynomial efficiently chosen based on the sample data whereas a Gaussian process interpolates the residuals (Couckuyt et al., 2013). The cross-validation plots in Fig. 7 show that the Blind-Kriging metamodels provide an accurate approximation of the outputs. Further explanation of Kriging models and the ooDACE toolbox is given in the Appendix B.

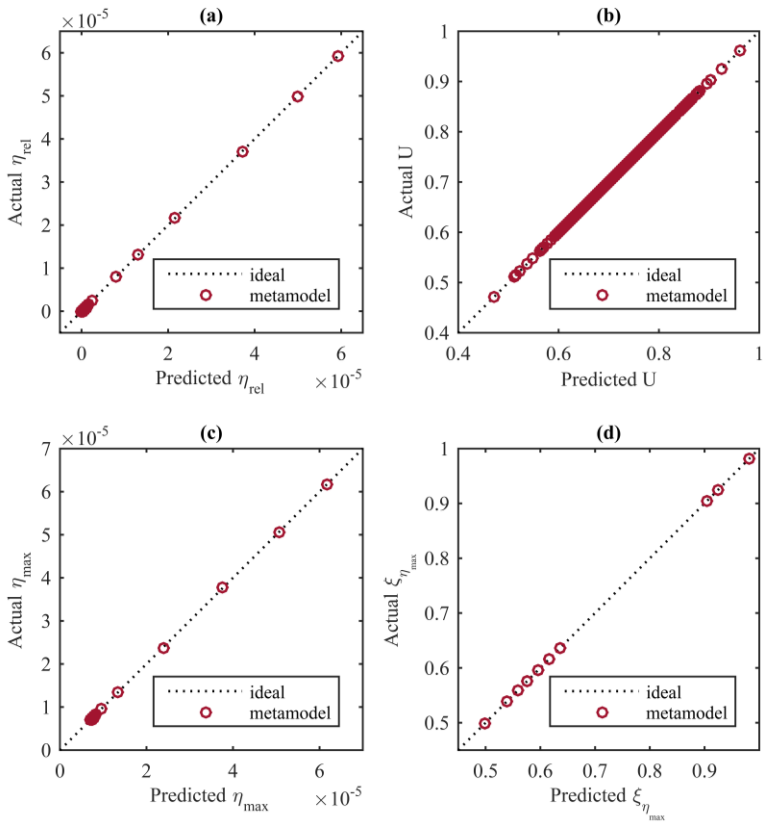

Fig. 7 Cross-validation plots of Kriging metamodels after 300 scenarios for (a) maximum relative dynamic buckling, (b) global usage factor, (c) maximum absolute dynamic buckling and (d) coordinate of maximum absolute dynamic buckling.

Fig. 8 presents the results after 1.5×10^6 MCSs. Random responses $\underline{\eta}_{rel}$ and $\underline{U}$ in Fig. 8(a) observe positive correlation which is also seen in Table 3.

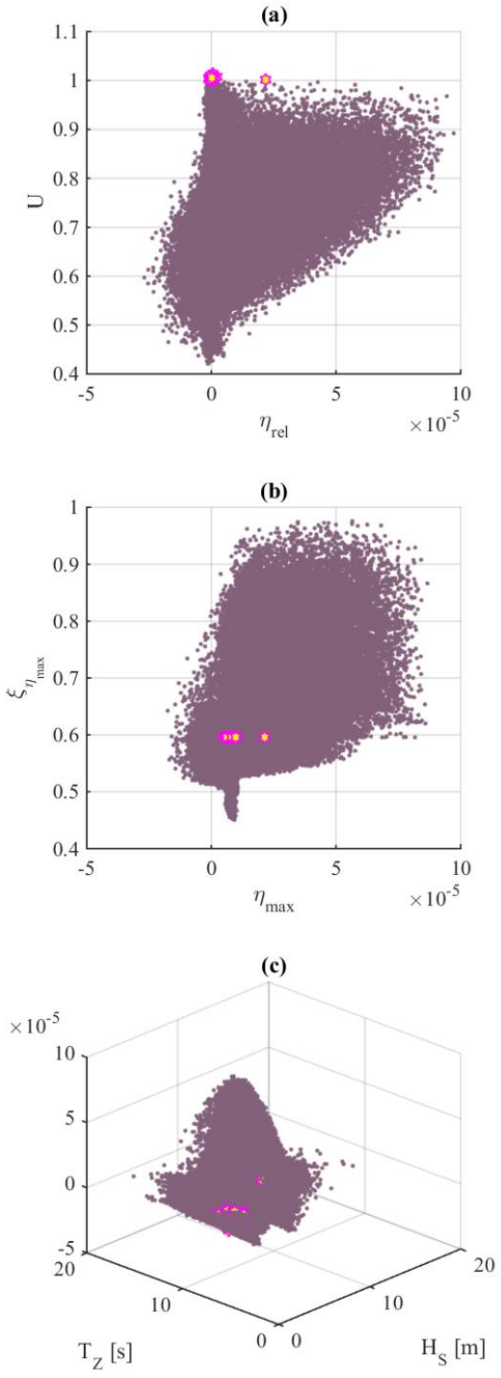

Fig. 8 Scatter plots after 1.5×10^6 MCSs: (a) maximum relative dynamic buckling vs. global usage factor, (b) maximum absolute dynamic buckling vs. its coordinate, and (c) maximum absolute dynamic buckling as function of significant wave height and zero-crossing wave period (dots represent non-failure events and magenta-yellow hexagrams represent failure events).

Table 3 Matrix of correlation coefficients

	$\underline{\eta}_{rel}$	$\underline{U}$	$\underline{\eta}_{\max}$	$\underline{\xi}_{\eta_{\max}}$	$\underline{H}_S$	$\underline{T}_Z$	$\underline{\rho}_i$	$\underline{k}$	$\underline{F}$	$\underline{\sigma}_y$	$\underline{\sigma}_u$
$\underline{\eta}_{rel}$	1.0000	0.1131	0.9742	0.4876	0.4169	0.2404	0.1050	-0.0237	-0.0428	0.0006	-0.0004
$\underline{U}$	0.1131	1.0000	0.0481	0.6149	0.0192	0.0176	0.9868	-0.0011	0.0277	-0.1190	-0.0596
$\underline{\eta}_{\max}$	0.9742	0.0481	1.0000	0.4240	0.3752	0.2274	0.0399	-0.0145	-0.0427	0.0004	-0.0005
$\underline{\xi}_{\eta_{\max}}$	0.4876	0.6149	0.4240	1.0000	0.2620	0.1281	0.6153	0.0240	-0.0884	-0.0001	-0.0005
$\underline{H}_S$	0.4169	0.0192	0.3752	0.2620	1.0000	0.6131	-0.0012	0.0001	-0.0005	0.0007	0.0010
$\underline{T}_Z$	0.2404	0.0176	0.2274	0.1281	0.6131	1.0000	0.0000	-0.0006	-0.0011	0.0005	0.0002
$\underline{\rho}_i$	0.1050	0.9868	0.0399	0.6153	-0.0012	0.0000	1.0000	0.0013	0.0001	0.0007	-0.0011
$\underline{k}$	-0.0237	-0.0011	-0.0145	0.0240	0.0001	-0.0006	0.0013	1.0000	-0.0007	-0.0008	-0.0006
$\underline{F}$	-0.0428	0.0277	-0.0427	-0.0884	-0.0005	-0.0011	0.0001	-0.0007	1.0000	-0.0004	-0.0006
$\underline{\sigma}_y$	0.0006	-0.1190	0.0004	-0.0001	0.0007	0.0005	0.0007	-0.0008	-0.0004	1.0000	-0.0007
$\underline{\sigma}_u$	-0.0004	-0.0596	-0.0005	-0.0005	0.0010	0.0002	-0.0011	-0.0006	-0.0006	-0.0007	1.0000

The variables representing the dynamic buckling, $\underline{\eta}_{rel}$ and $\underline{\eta}_{\max}$, observe positive correlation with the sea wave parameters $\underline{H}_S$ and $\underline{T}_Z$. It is detected that the usage factor $\underline{U}$ is strongly influenced by $\underline{\rho}_i$. An interesting result is that $\underline{U}$ is positively correlated with the location of the maximum buckling response $\underline{\xi}_{\eta_{\max}}$.

The calculated probabilities of dynamic buckling P_B and of failure P_f are listed in Table 4. While the dynamic buckling is expected to occur quite often, the value of P_f is acceptable for structures with normal relative effort to achieve reliability and large expected failure consequences (Rackwitz, 2000). Of course, this approach can be useful to evaluate the dynamic buckling-based reliability of a riser under design.

Table 4 Calculated probabilities

P_B	P_f	$P_B \cap P_f$	$P_{f\|B}$
7.816×10^{-1}	1.5333×10^{-5}	8.6667×10^{-6}	1.1089×10^{-5}

Fig. 9 shows the approximate PDFs of input variables and relative dynamic buckling between its full population and failure scenarios by using the ksdensity function available in Matlab. From the results, it can be said that failure is likely to occur in scenarios with high internal fluid's density and internal overpressure [Fig. 9(c)], high stiffness of tensioning system [Fig. 9(d)], and low material strength [Fig. 9(f) and (g)].

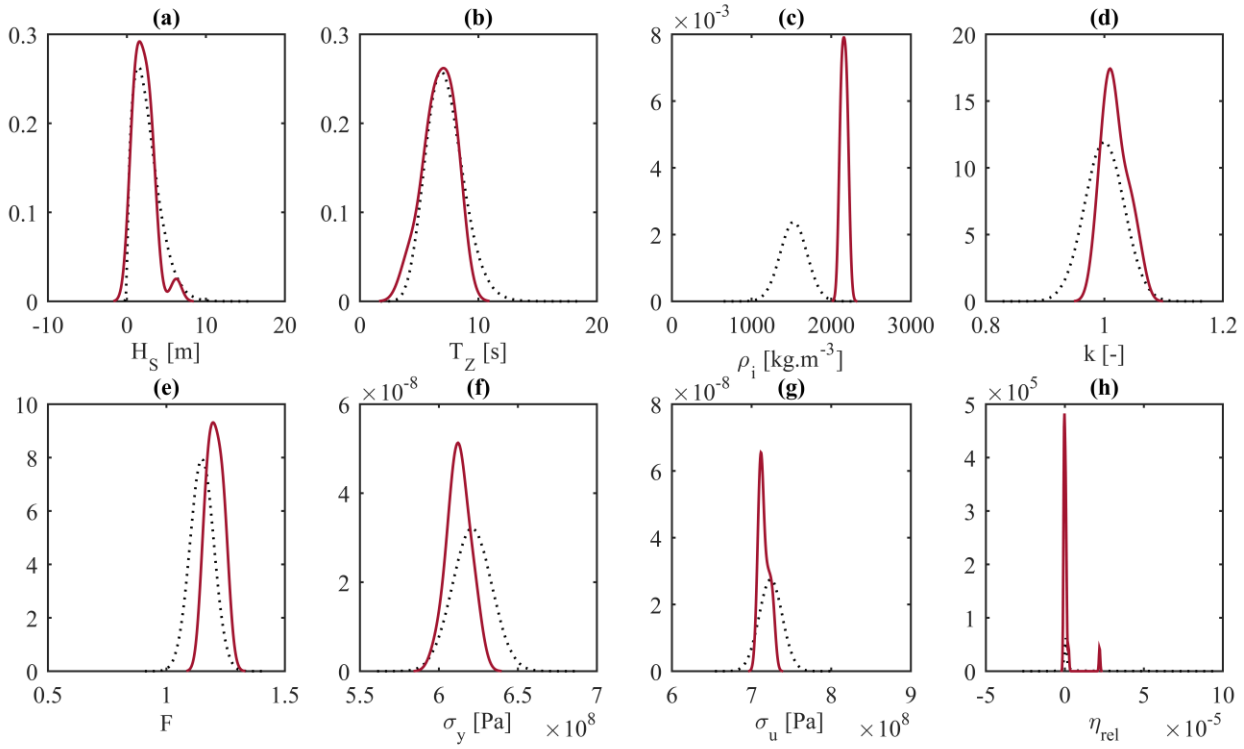

Fig. 9 PDFs of random variables: black dotted line represents the long-term distribution (based on 1.5×106 MCSs) and red solid line represents distribution at failure (based on 23 MCSs with failure).

5.2 Effect of top-tension

The influence of the minimum top-tension factor F in association with the probabilities of dynamic buckling and failure is further investigated. From the negative correlation coefficient between $\underline{F}$ and $\underline{\eta}_{rel}$ in Table 3, it is anticipated that high top-tension would reduce the dynamic buckling response.

The effect of $\underline{F}$ in the probability of failure is more complex. Table 3 and Fig. 9(e) indicate that failure events are associated with high F due to the increase of tensile loads and hence it might be desirable to reduce the static top-tension. On the other hand, Fig. 10 shows that the pretension factor f defined in Eq. (7) becomes less than one for low F, which means that the top-tension is less than the effective weight and thus part the riser's body is under negative effective tension.

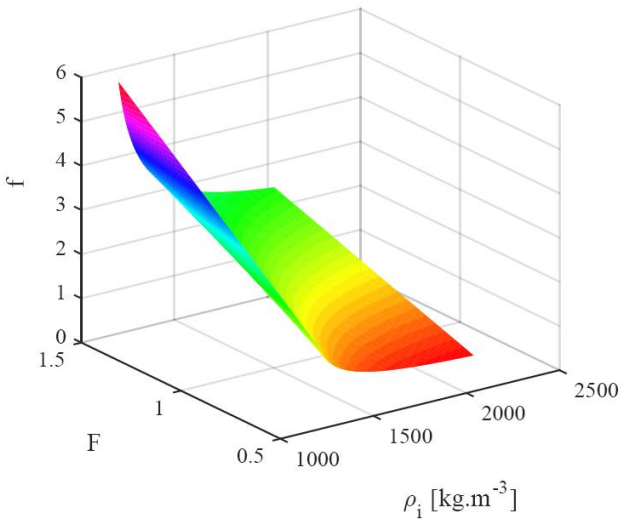

Fig. 10 Pretension factor f as function of internal fluid's density and minimum top-tension factor.

To illustrate the effect of negative effective tension, Fig. 11 presents the results for the time-domain analysis of a riser when F =0.4, (other parameters the same as for Fig. 3). Fig. 11(a) and (b) show that the transverse deflection grows with time. Fig. 11(b) displays that the nodal velocity oscillates due to the random excitation. The maximum deformation at the end of the simulation in Fig. 11(a) and (c) is in the order of η =1400 (4.2×10^6 m), which clearly violates the classical condition of small transverse deflection in which the governing Eq. (1) is founded. The associated global usage is U =416.46 which is dominated by the large buckling-induced bending moment.

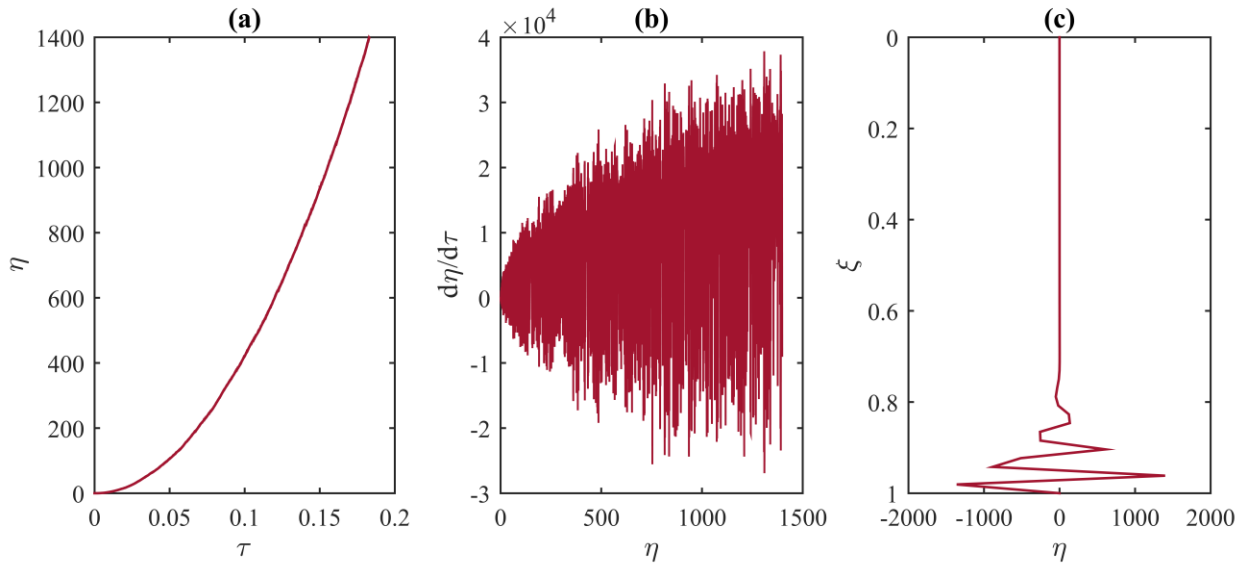

Fig. 11 Evolution of dynamic buckling with low top-tension for F =0.4, f =0.7505, H_S =10.13 m, ω_p =0.3972 rad·s^{-1}, ρ_i =1 600 kg·m^{-3}: (a) time history of transverse deflection at at ξ =0.9615, (b) phase portrait of riser motion at ξ =0.9615, and (c) deformed shape at the end time of analysis.

The procedure in Fig. 6 is applied anew with evaluation rules to account for scenarios with f <1. The random variables in Table 2 are employed, except that the minimum top-tension factor F is taken as a deterministic variable and $\underline{\rho}_i$ is assumed to be uniformly distributed between 1200 and 2037 kg·m^{-3}.

For the LHS, another 300 scenarios are sampled, where F is uniformly distributed between 0.2 and 1.5. Then Blind-Kriging metamodels for η_{rel} and U are computed from 226 scenarios while 74 scenarios are neglected in order to avoid strong discontinuities in the approximate functions.

During the MCS, two rules are included. If f <1, η_{rel} is automatically set to a value larger than 0 to indicate that buckling occurs, and U is set to a value larger than 1 in order to account for failure under large transversal deflection.

The results are presented in Fig. 12. It can be seen that the probability of dynamic buckling approaches to 1 as the top-tension is reduced. It is seen that the probability of failure is high for too low values of F, because the top-tension is insufficient to keep the riser's straight shape, and it is also high for large F because of failure under high tension. It is also observed that the discontinuity in the results at F =0.6 is consistent with the occurrence of f <1 in Fig. 10.

In view of the results, the operation of riser as recommended by API RP 16Q (American Petroleum Institute, 2017), namely using F =1, is adequate to account for the phenomenon of dynamic buckling. The probability of failure can even be even reduced

during the operation of disconnectable systems, while it cannot be modified for permanent risers. It should be mentioned that this study is for a riser in calm water. For a comprehensive analysis, more complex fluid-structure interactions with waves and currents should be accounted for; also soil-structure interaction and floater motions in more degrees of freedom should be accounted for the global riser response.

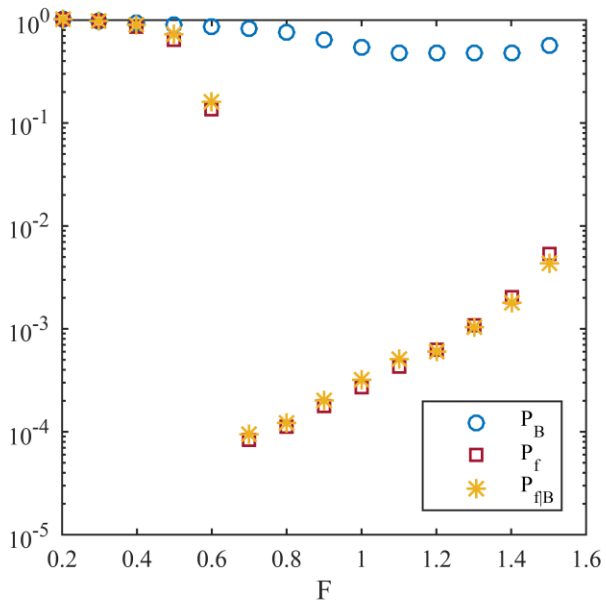

Fig. 12 Probabilities of dynamic buckling, failure and conditional as function of minimum top-tension factor (each set of three points corresponds to 1.5×10^{6} MCSs).

6. Concluding remarks

The aim of the present work has been to investigate the stochastic heave-induced dynamic buckling in a top-tensioned riser and its effect on the probability of failure. The governing differential equation of motion for the riser with nonlinear damping

was derived and solved by means of the finite difference method together with a Runge-Kutta method for time integration. The evolution of the riser's motion showed that the dynamic buckling response is bounded by the presence of quadratic damping. Then, a map of maximum absolute response was used to identify the sea wave parameters that may cause dynamic buckling. It shows that dynamic buckling develops in sea states with high significant wave height and low peak circular frequency.

The dynamic buckling was studied as a random process which is excited by a floater with random heave motion. Long-term random variables were characterized by means of their probability density functions. Implementation of the MCS method allowed to compute the probability of dynamic buckling (7.816×10^{-1}) and the probability of failure given dynamic buckling (1.1089×10^{-5}) for an applied example, and then to investigate the influence of reducing the top-tension.

In view of the results, dynamic buckling is certainly expected to occur in a top-tensioned riser, but the probability of failure can of course be kept under an acceptable safety level associated with an ultimate limit state.

It can be said that the present study achieves its objectives. Further improvements of the proposed methodology comprise the use sequential design of experiments instead of one shot LHS designs [see for example Kleijnen (2017)], and the use of nonlinear formulations to account to the riser's top-tension [see for example Guimarães Pestana et al. (2016)].

Regarding future research, it is desirable to understand the phenomenon of heave-induced dynamic buckling by accounting to more nonlinearities such as riser's

extensibility, large transversal deformations and nonlinear boundary conditions. In this regard, it is recommended to investigate the fluid-structure interaction between the riser and the surrounding fluid by means of 3D nonlinear finite element method. Moreover, since it is expected that heave-induced dynamic buckling would occur often throughout the riser's life, it is suggested to study its effect in the fatigue limit state reliability. The reliability of the riser during accidental conditions, such as tensioners lock-off or sudden loss of top-tension are also recommended for further study.

Acknowledgements

This study was undertaken at the Korea Ship and Offshore Research Institute at Pusan National University which has been a Lloyd's Register Foundation Research Centre of Excellence since 2008. This work was supported by a 2-Year Research Grant of Pusan National University. The first author would like to acknowledge the scholarship from the Mexican National Council for Science and Technology (CONACYT).

Appendix A. Finite difference formulation

In relation with the riser's governing equation and following the same strategy as others (Kuiper et al., 2008), it is convenient to introduce the following dimensionless variables:

$$\begin{aligned}&\eta = w/L, \xi = z/L, \tau = t\sqrt{EI/M}\,/L^2, \alpha = W_e L^3/(EI), \chi(\tau) = \kappa Z(\tau)/a_c,\\ &\mu = C_d \rho_f DL/(2M), \kappa_1 = k_2 L/(EI), \kappa_2 = k_3 L/(EI).\end{aligned} \tag{A1}$$

Substituting the effective tension of Eq. (3) and employing previous dimensionless variables, the governing Eq. (1) may be rewritten as

$$\frac{\partial^4\eta}{\partial\xi^4}+\alpha\left(\xi-f\right)\frac{\partial^2\eta}{\partial\xi^2}+\alpha\chi\left(\tau\right)\frac{\partial^2\eta}{\partial\xi^2}+\alpha\frac{\partial\eta}{\partial\xi}+\frac{\partial^2\eta}{\partial\tau^2}+\mu\left|\frac{\partial\eta}{\partial\tau}\right|\frac{\partial\eta}{\partial\tau}=0,\qquad 0\le\xi\le 1, \tag{A2}$$

and the boundary conditions (2) become

$$\begin{aligned}&\eta\left(0,\tau\right)=0,\\&\left.\frac{\partial^2\eta\left(\xi,\tau\right)}{\partial\xi^2}\right|_{\xi=0}=\kappa_1\left.\frac{\partial\eta\left(\xi,\tau\right)}{\partial\xi}\right|_{\xi=0},\\&\eta\left(1,\tau\right)=0,\\&\left.\frac{\partial^2\eta\left(\xi,\tau\right)}{\partial\xi^2}\right|_{\xi=1}=-\kappa_2\left.\frac{\partial\eta\left(\xi,\tau\right)}{\partial\xi}\right|_{\xi=1}.\end{aligned} \tag{A3}$$

To solve Eq. (A2), the space ξ is discretized into $N+1$ interior mesh points, each designated by $i=0,1,2,...,N$ and equally spaced with step $h=1/N$. Using a central difference approximation, the derivatives are estimated as follows:

$$\begin{aligned}\left.\frac{\partial\eta\left(\xi,\tau\right)}{\partial\xi}\right|_{\xi=\xi_i}&\approx\frac{\eta_{i+1}-\eta_{i-1}}{2h},\\\left.\frac{\partial\eta^2\left(\xi,\tau\right)}{\partial\xi^2}\right|_{\xi=\xi_i}&\approx\frac{\eta_{i+1}-2\eta_i+\eta_{i-1}}{h^2},\\\left.\frac{\partial\eta^4\left(\xi,\tau\right)}{\partial\xi^4}\right|_{\xi=\xi_i}&\approx\frac{\eta_{i+2}-4\eta_{i+1}+6\eta_i-4\eta_{i-1}+\eta_{i-2}}{h^4},\end{aligned} \tag{A4}$$

where η_i denotes the nodal value at the i-th node with coordinate $\xi_i=ih$.

Substitution of Eq. (A4) into Eq. (A2) yields the finite difference equation

$$\frac{\eta_{i+2}-4\eta_{i+1}+6\eta_i-4\eta_{i-1}+\eta_{i-2}}{h^4}+\alpha\left(\xi_i-f\right)\frac{\eta_{i+1}-2\eta_i+\eta_{i-1}}{h^2}$$
$$+\alpha\chi\left(\tau\right)\frac{\eta_{i+1}-2\eta_i+\eta_{i-1}}{h^2}+\alpha\frac{\eta_{i+1}-\eta_{i-1}}{2h}+\frac{\partial^2\eta}{\partial\tau^2}+\mu\left|\frac{\partial\eta_i}{\partial\tau}\right|\frac{\partial\eta_i}{\partial\tau}=0, \qquad \text{(A5)}$$
$$i=0,1,2,...,N.$$

Likewise, substitution of Eq. (A4) into the boundary conditions Eq. (A3) gives the following nodal values:

$$\begin{aligned}&\eta_0=0,\\&\eta_{-1}=\frac{\eta_1\left(h\kappa_1-2\right)}{h\kappa_1+2},\\&\eta_N=0,\\&\eta_{N+1}=\frac{\eta_{N-1}\left(h\kappa_2-2\right)}{h\kappa_2+2}.\end{aligned} \qquad \text{(A6)}$$

To integrate the system (A5), it is first necessary to rewrite it into a state-space form. This is achieved by letting η_j for $j=-1,0,1,2,...,N-1,N,N+1$ become $\eta_j=x_i$ for odd i; and its derivatives become $d\eta_j/d\tau=x_i$ for even i.

As a result, the following system of first order ordinary nonlinear equations is obtained:

$$
\dot{x}_i = \begin{cases} x_{i+1}, & i = 1, 3, ..., 2(N-1)-1 \\ -\dfrac{1}{h^4} x_{i-5} + \left(\dfrac{4}{h^4} + \dfrac{\alpha f}{h^2} - \dfrac{\alpha \xi_i}{h^2} - \dfrac{\alpha \chi(\tau)}{h^2} + \dfrac{\alpha}{2h} \right) x_{i-3} & \\ + \left(\dfrac{2\alpha \xi_i}{h^2} - \dfrac{2\alpha f}{h^2} + \dfrac{2\alpha \chi(\tau)}{h^2} - \dfrac{6}{h^4} \right) x_{i-1} & i = 2, 4, ..., 2(N-1) \\ + \left(\dfrac{4}{h^4} + \dfrac{\alpha f}{h^2} - \dfrac{\alpha \xi_i}{h^2} - \dfrac{\alpha \chi(\tau)}{h^2} - \dfrac{\alpha}{2h} \right) x_{i+1} - \dfrac{1}{h^4} x_{i+3} - \mu |x_i| x_i, & \end{cases}
$$

$$
i = 1, 2, ..., 2(N-1),
$$

$$
x_{-3} = \frac{x_1 (h\kappa_1 - 2)}{h\kappa_1 + 2},
$$

$$
x_{-1} = 0, \tag{A7}
$$

$$
x_{2N-1} = 0,
$$

$$
x_{2N+1} = \frac{x_{2N-3} (h\kappa_2 - 2)}{h\kappa_2 + 2},
$$

$$
\xi_i = ih/2,
$$

where the overdot denotes the derivative respect to the dimensionless time τ, and x_i represents nodal displacements and velocities for odd i and even i, respectively. This system is then solved by means of a Runge-Kutta method.

Appendix B. Kriging models with the ooDACE toolbox

A Kriging model is a Gaussian process interpolation-based metamodel or surrogate model which assumes the form of (Couckuyt et al., 2013)

$$
y(\mathbf{x}) = g(\mathbf{x}) + Z(\mathbf{x}) \tag{B1}
$$

where $\mathbf{x}$ is the vector of input variables, $g(\mathbf{x})$ is a regression function interpreted as the mean of the broader Gaussian process $y(\mathbf{x})$, $Z(\mathbf{x})$ is a Gaussian process with zero

mean and covariance function $\mathrm{Cov}\left[Z(\mathbf{x}), Z(\mathbf{x}')\right] = \sigma^2 \mathrm{R}(\mathbf{x}, \mathbf{x}', \boldsymbol{\varphi})$ (Fang et al., 2006, Chapter 1), σ^2 is the unknown variance of $Z(\mathbf{x})$, R is a correlation function between $\mathbf{x}$ and $\mathbf{x}'$, and $\boldsymbol{\varphi}$ is a set of correlation parameters used to fit the model. Additionally, unknown parameters $\boldsymbol{\beta}$ are required to fit the regression function.

Parameters $\boldsymbol{\beta}$, σ^2 and $\boldsymbol{\varphi}$ are to be determined from computer experiments (simulations) with design (input) $X = \{\mathbf{x}_1, ..., \mathbf{x}_m\}$ and responses $Y = \{y_1, ..., y_m\}$ (Martínez-Frutos and Martí, 2014), where the design of experiments is usually carried out by means of Latin hypercube sampling (LHS). Said sampling technique is recommended since it provides data from large experimental areas by dividing the range of each input into several mutually exclusive and exhaustive intervals of equal probability (Kleijnen, 2017).

One of the tools to compute Kriging models is the ooDACE toolbox (Couckuyt et al., 2012, 2010) developed at Gent University which allows not only to compute Ordinary Kriging metamodels, but also numerous variants depending on the type of regression function. For instance, it supports Simple, Ordinary and Universal Kriging models with known constant, unknown constant or unknown polynomial function, respectively (Ulaganathan et al., 2015). Furthermore, as the selection of the regression function is often difficult, it can also perform Blind Kriging, in which the regression function is chosen to capture the most variance in the sample data by means of Bayesian approximations (Couckuyt et al., 2012). Other features of the tool are the use of Stochastic Kriging and Gradient Kriging models.

References

American Petroleum Institute, 2017. Design, Selection, Operation, and Maintenance of Marine Drilling Riser Systems API Recommended Practice 16Q, Second. ed. Washington, DC.

American Petroleum Institute, 2004. Specification for Line Pipe API Specification 5L, Forty-thir. ed. API Publishing Services, Washington, D.C.

Benettin, G., Galgani, L., Giorgilli, A., Strelcyn, J.-M., 1980a. Lyapunov Characteristic Exponents for smooth dynamical systems and for Hamiltonian systems; a method for computing all of them. Part 1: Theory. Meccanica 15(1), 9–20.

Benettin, G., Galgani, L., Giorgilli, A., Strelcyn, J.M., 1980b. Lyapunov Characteristic Exponents for smooth dynamical systems and for hamiltonian systems; A method for computing all of them. Part 2: Numerical application. Meccanica 15(1), 21–30.

Cabrera-Miranda, J.M., Paik, J.K., 2017. On the probabilistic distribution of loads on a marine riser. Ocean Eng. 134, 105–118.

Chatjigeorgiou, I.K., 2004. On the parametric excitation of vertical elastic slender structures and the effect of damping in marine applications. Appl. Ocean Res. 26(1-2), 23–33.

Chatjigeorgiou, I.K., Mavrakos, S.A., 2005. Nonlinear resonances of parametrically excited risers-numerical and analytic investigation for Ω = 2ω1. Comput. Struct. 83(8-9), 560–573.

Chatjigeorgiou, I.K., Mavrakos, S.A., 2002. Bounded and unbounded coupled

transverse response of parametrically excited vertical marine risers and tensioned cable legs for marine applications. Appl. Ocean Res. 24(6), 341–354.

Clauss, G., Lehmann, E., Östergaard, C., 1992. Offshore Structures: Volume I: Conceptual Design and Hydromechanics. Springer-Verlag London Limited, London.

Couckuyt, I., Declercq, F., Dhaene, T., Rogier, H., Knockaert, L., 2010. Surrogate-based infill optimization applied to electromagnetic problems. Int. J. RF Microw. Comput. Eng. 20(5), 492–501.

Couckuyt, I., Dhaene, T., Demeester, P., 2013. ooDACE toolbox, A Matlab Kriging toolbox: Getting started [WWW Document]. URL http://sumo.intec.ugent.be/?q=ooDACE (accessed 7.15.16).

Couckuyt, I., Forrester, A., Gorissen, D., De Turck, F., Dhaene, T., 2012. Blind Kriging: Implementation and performance analysis. Adv. Eng. Softw. 49, 1–13.

Det Norske Veritas, 2010. Offshore Standard DNV-OS-F201 Dynamic Risers. Høvik, Norway.

Det Norske Veritas AS, 2014. Recommended practice DNV-RP-C205, Environmental Conditions and Environmental Loads. Høvik, Norway.

DNV GL, 2016. World Offshore Accident Database [WWW Document]. URL http://woad.dnv.com (accessed 8.26.16).

Fang, K., Li, R.Z., Sudjianto, A., 2006. Design and modeling for computer experiments, Computer Science and Data Analysis Series. Chapman & Hall/CRC, Boca Raton, FL, USA.

Forghani, S.M., Ritto, T.G., 2016. Stochastic stability of the non-homogeneous damped Mathieu equation. Nonlinear Dyn. 86, 1561–1570.

Franzini, G.R., Mazzilli, C.E.N., 2016. Non-linear reduced-order model for parametric excitation analysis of an immersed vertical slender rod. Int. J. Non. Linear. Mech. 80, 29–39.

Franzini, G.R., Pesce, C.P., Salles, R., Gonçalves, R.T., Fujarra, A.L.C., Mendes, P., 2015. Experimental Analysis of a Vertical and Flexible Cylinder in Water : Response to Top Motion Excitation and Parametric Resonance. J. Vib. Acoust. 137(3), 31010-1-31010–12.

Garrè, L., Rizzuto, E., 2012. Bayesian networks for probabilistic modelling of still water bending moment for side-damaged tankers. Ships Offshore Struct. 7(3), 269–283.

Guimarães Pestana, R., Edward Roveri, F., Franciss, R., Bruno Ellwanger, G., 2016. Marine riser emergency disconnection analysis using scalar elements for tensioner modelling. Appl. Ocean Res. 59, 83–92.

Hsu, C.S., 1975. The response of a parametrically excited hanging string in fluid. J. Sound Vib. 39(3), 305–316.

Institut Français du Pétrole, 1999. Drilling data handbook, Seventh. ed. Éditions Technip, Paris.

ISO, 2009. ISO/TR 13624-2 Petroleum and natural gas industries — Drilling and production equipment — Part 2: Deepwater drilling riser methodologies, operations, and integrity technical report. International Organization for Standarization, Geneva,

Switzerland.

Katifeoglou, S.A., Chatjigeorgiou, I.K., 2016. Dynamics of shell-like tubular segments at the sagbend region of a steel catenary riser. Ships Offshore Struct. 11(8), 860–873.

Kleijnen, J.P.C., 2017. Regression and Kriging metamodels with their experimental designs in simulation: A review. Eur. J. Oper. Res. 256, 1–16.

Kucheryavyi, V.I., Milkov, S.N., 2014. Strength Reliability of Gas-Supply Pipes of Large Diameter. J. Mach. Manuf. Reliab. 43(5), 448–452.

Kuiper, G.L., Brugmans, J., Metrikine, A. V., 2008. Destabilization of deep-water risers by a heaving platform. J. Sound Vib. 310(3), 541–557.

Lei, S., Zhang, W.S., Lin, J.H., Yue, Q.J., Kennedy, D., Williams, F.W., 2014. Frequency domain response of a parametrically excited riser under random wave forces. J. Sound Vib. 333(2), 485–498.

Li, X., Guo, H., Meng, F., 2010. Stress analysis of top tensioned riser under random waves and vessel motions. J. Ocean Univ. China 9, 251–256.

Lu, J., Yang, G., Oh, H., Luo, A.C.J., 2005. Computing Lyapunov exponents of continuous dynamical systems: Method of Lyapunov vectors. Chaos, Solitons and Fractals 23(5), 1879–1892.

Martínez-Frutos, J., Martí, P., 2014. Diseño óptimo robusto utilizando modelos Kriging: Aplicación al diseño óptimo robusto de estructuras articuladas. Rev. Int. Métodos Numéricos para Cálculo y Diseño en Ing. 30, 97–105. [in Spanish]

Mazzilli, C.E.N., Rizza, F., Dias, T., 2016. Heave-imposed motion in vertical risers: a

reduced-order modelling based on Bessel-like modes. Procedia IUTAM 19, 136–143.

Nayfeh, A.H., Balachandran, B., 2004. Applied Nonlinear Dynamics: Analytical, Computational, and Experimental Methods. WILEY-VCH Verlag GMbH & Co. KGaA, Weinheim.

Nayfeh, A.H., Mook, D.T., 1995. Nonlinear Oscillations, Wiley Clas. ed. John Wiley & Sons, Inc., New York.

Paik, J.K., Thayamballi, A.K., 2003. Ultimate Limit State Design of Steel-Plated Structures. John Wiley & Sons Ltd, West Sussex, England.

Park, H.I., Jung, D.H., 2002. A finite element method for dynamic analysis of long slender marine structures under combined parametric and forcing excitations. Ocean Eng. 29(11), 1313–1325.

Patel, M.H., Park, H.I., 1995. Combined axial and lateral responses of tensioned buoyant platform tethers. Eng. Struct. 17(10), 687–695.

Patel, M.H., Park, H.I., 1991. Dynamics of tension leg platform tethers at low tension. Part I - Mathieu stability at large parameters. Mar. Struct. 4(3), 257–273.

Patel, M.H., Vaz, M.A., 1996. On the mechanics of submerged vertical slender structures subjected to varying axial tension. Philos. Trans. Math. Phys. Eng. Sci. 354, 609–648.

Patel, M.H., Witz, J.A., 1991. Compliant Offshore Structures. Butterworth-Heinemann Ltd, Oxford.

Permana, W.E., 2012. A Comparative Analysis of 21 inch and 16 inch Drilling Riser for Deepwater Application (Master's Thesis). University of Stavanger, Stavanger.

Pipchenko, A.D., 2009. On the method of calculation of ship's transverse stability in regular waves. Ships Offshore Struct. 4(1), 9–18.

Prado, F.S., Sakamoto, F.Y., Mazzilli, C.E.N., 2014. An analysis of parametric instability of risers. Lat. Am. J. Solids Struct. 11(3), 348–368.

Rackwitz, R., 2000. Optimization — the basis of code-making and reliability verification. Struct. Saf. 22(1), 27–60.

Sarpkaya, T., 2010. Wave Forces on Offshore Structures. Cambridge University Press, Cambridge, UK.

Shimada, I., Nagashima, T., 1979. A Numerical Approach to Ergodic Problems of Dissipative Dynamical Systems. Prog. Theor. Phys. 61(6), 1605–1616.

Thomas, G., Duffy, J., Lilienthal, T., Watts, R., Gehling, R., 2010. On the avoidance of parametric roll in head seas. Ships Offshore Struct. 5(4), 295–306.

Ulaganathan, S., Couckuyt, I., Deschrijver, D., Laermans, E., Dhaene, T., 2015. A Matlab toolbox for Kriging metamodelling. Procedia Comput. Sci. 51, 2708–2713.

Wang, Y., Gao, D., Fang, J., 2015. Coupled dynamic analysis of deepwater drilling riser under combined forcing and parametric excitation. J. Nat. Gas Sci. Eng. 27, 1739–1747.

Wu, Z.W., Liu, J.K., Liu, Z.Q., Lu, Z.R., 2016. Parametrically excited vibrations of marine riser under random wave forces and earthquake. Adv. Struct. Eng. 19(3), 449–462.

Xiao, F., Yang, H.Z., 2014. Probabilistic assessment of parametric instability of a top tensioned riser in irregular waves. J. Mar. Sci. Technol. 19(3), 245–256.

Yang, H., Wang, Z., Xiao, F., 2017. Parametric resonance of submerged floating pipelines with bi-frequency parametric and vortex-induced oscillations excitations. Ships Offshore Struct. 12(3), 395–403.

Yang, H., Xiao, F., 2014. Instability analyses of a top-tensioned riser under combined vortex and multi-frequency parametric excitations. Ocean Eng. 81, 12–28.

Yang, H., Xiao, F., Xu, P., 2013. Parametric instability prediction in a top-tensioned riser in irregular waves. Ocean Eng. 70, 39–50.

Yang, H.Z., Zheng, W., 2011. Metamodel approach for reliability-based design optimization of a steel catenary riser. J. Mar. Sci. Technol. 16(2), 202–213.

Zhang, J., Tang, Y., 2015. Parametric Instability Analysis of Deepwater Top-Tensioned Risers Considering Variable Tension Along the Length. J. Ocean Univ. China 14(1), 59–64.

Zio, E., 2013. Monte Carlo Simulation: The Method, in: The Monte Carlo Simulation Method for System Reliability and Risk Analysis. Springer, London, pp. 19–58.